Optics and Lasers in Engineering 150 (2022) 106843

Contents lists available at ScienceDirect

Optics and Lasers in Engineering

journal homepage: www.elsevier.com/locate/optlaseng

Deep learning colorful ptychographic iterative engine lens-less diffraction microscopy

Yinxu Bian[a], Yannan Jiang[b], Jiaxiong Wang[c], Shenmin Yang[c], Weijie Deng[d,e], Xiaofei Yang[f], Renbing Shen[b], Hua Shen[a,g,*], Cuifang Kuang[h,i,*]

[a] School of Electronic and Optical Engineering, Nanjing University of Science and Technology, Nanjing, 210094, P.R. China
[b] Department of General Surgery, The Affiliated Suzhou Hospital of Nanjing Medical University, Suzhou Municipal Hospital, Suzhou, 215002, P.R. China
[c] Center of Reproduction and Genetics, Affiliated Suzhou Hospital of Nanjing Medical University, Suzhou Municipal Hospital, Suzhou, 215002, P.R. China
[d] Changchun Institute of Optics, Fine Mechanics and Physics, Chinese Academy of Sciences, Changchun, 130033, P.R. China
[e] Key Laboratory of Optical System Advanced Manufacturing Technology, Chinese Academy of Sciences, Changchun, 130033, P.R. China
[f] School of Optoelectronic Science and Engineering & Collaborative Innovation Center of Suzhou Nano Science and Technology, Soochow University, Suzhou, 215006, P.R. China
[g] Department of Material Science and Engineering, University of California Los Angeles, Los Angeles, CA, 90095, United States of America
[h] State Key Laboratory of Modern Optical Instrumentation, Zhejiang University, Hangzhou, 310027, P.R. China
[i] College of Optical Science and Engineering, Zhejiang University, Hangzhou, 310027, P.R. China

ARTICLE INFO

Keyword:
Computational imaging
Ptychographic iterative engine (PIE)
Lens-less microscopy
Deep learning

ABSTRACT

The ptychographic iterative engine (PIE) is an algorithm for coherent lens-less diffraction imaging. It facilitates the development of low-cost large field of view (FOV) lens-less microscopy, as it can expand the FOV extensively by moving the light source or the bio-medical pathological sample slide. In a PIE setup, the illumination light needs to have high/partially coherence. Thus, to get a colorful microscopy image, more than 3 illumination light sources with different dominant wavelengths are required in a traditional PIE setup. In this manuscript, an improved PIE based on computational deep learning color-transferring method is proposed to achieve colorful large FOV lens-less microscopy imaging. In our method, only one high/partially coherent light source is used, where the image data are three times less than those images under multiple illuminations for colorful PIE microscopy. It is believable that our colorful PIE microscopy enhanced by the deep color-transferring method would be helpful for the development of low-cost large FOV lens-less microscopes.

1. Introduction

Large field-of-view (FOV) and high-resolution microscopy imaging is indispensable for bio-medical pathological slide observing and diagnosing. In a research-level biological center or hospital, these microscopy diagnosis demands would be realized by commercial bench-top microscopes. However, commercial bench-top microscopes are limited resources in the villages and remote areas. In recent years, lens-less microscopy based on coherent diffraction imaging (CDI) [1–6] attracts researchers to develop low-cost portable and light-weight microscopes [7–12]. Under high/partial coherent light illumination, CDI setups would retrieve the complex wavefront, including the amplitude and the phase. And lenses and complex optical components are not necessary in these setups. Ptychographic iterative engine (PIE) [11,12] lens-less microscopy is a kind of coherent diffraction imaging (CDI) methods. In contrast to other CDI algorithms, e.g., Gerchberg-Saxton (G-S) algorithms [7–10], transport-of-intensity phase retrieval algorithms [13] and so on [14–20], PIE would extend the FOV [9,11,12]. In the aspect of hardware, PIE scans the thin bio-sample slide in a 2-dimension (2D) plane, which is perpendicular to the optical axis. Simultaneously, the diffraction images are recorded by a digital CCD/CMOS image sensor. In the aspect of image reconstruction algorithms, the iterative updating computational formulas based on the Fresnel/Fraunhofer angular spectrum propagation are executed according to the recorded diffraction images stacks [16–20]. Thus, PIE has an outstanding advantage of achieving an amazingly large FOV lens-less microscopy, which theoretically has an infinite FOV by extensively scanning the thin bio-sample slide in a 2D plane. These advantages show the potentials to develop an extensible large FOV low-cost portable lens-less microscopes.

However, in contrast to the conventional lens-based bench-top bright-field microscopes, PIE microscopy could not provide a colorful image under only one high/partially coherent light illumination. To get a RGB color format image, more than three kinds of light illuminations are necessary. In clinical bio-medical pathological standard diagnosis

* Corresponding authors.
E-mail addresses: edward_bayun@163.com (H. Shen), cfkuang@zju.edu.cn (C. Kuang).

https://doi.org/10.1016/j.optlaseng.2021.106843
Received 13 June 2021; Received in revised form 23 September 2021; Accepted 7 October 2021
Available online 16 October 2021
0143-8166/

applications, chemical dying has been a popular method to label different areas of the tissue/cells. Besides, chemical dying tissue/cells slides would be sealed by wax for very long time, which could be helpful for conserving the typical bio-medical pathological samples. Thus, for these clinical standard diagnosis, RGB colorful microscopy imaging is attractive to doctors and biological researchers by the using of a low-cost portable PIE lens-less microscope.

In this manuscript, the deep learning color-transferring method is proposed to enhance the PIE microscopy for virtually colorizing, only with one high/partially coherent light illumination. Usually, bio-medical pathological tissues/cells slices are stained by gold-standard chemically dying. Thus, as limited artificially rendering, the colors of the chemically stained pathological tissues/cells in RGB images are less and simpler than those in natural scene digital photos. For example, hematoxylin and eosin (H&E) dying is widely adopted in pathological histology rendering and medical diagnosis. In H&E dyed pathological tissues/cells, the purplish-blue appearance regions represent the cell nucleuses, and pink appearance regions are the cellular matrix and cytoplasm parts. This means that color information relates with the morphological characteristics. Thus, it is probable that the chromatic greyscale PIE images under only one kind illumination could be virtually translated into the RGB colorful images, which we call colorful PIE. We believe that this colorful PIE would promote the development of the low-cost and portable large FOV lens-less microscopes.

In the following contents, firstly, the material and experimental setups are presented and described. Secondly, computational algorithms, including PIE and deep leaning image-style-transfer are stated. Thirdly, the experiments and data are present to show the effectiveness of our colorful PIE method.

2. Setup and material

As shown in Fig. 1, here we use a Fresnel domain propagation framework to achieve our extensible FOV PIE microscopy. In Fig. 1, partially coherent quasi-plane visible-light wave illuminates a circular aperture. The partially coherent light comes from a green (G) LED, which is coupled into a multi-mode quartz optical fiber. The partially coherent light emits from the other end of the quartz optical fiber. The distance between the circular aperture and the exit end of optical fiber is ~150 mm, named as L_1. After the circular aperture, the chemically dyed pathological tissue slides are fixed on a 2D moveable mechanical supporter. After the chemically dyed pathological tissue slides, a chromatic digital CMOS image sensor is used to record the diffraction images. The pathological tissue is fixed on a standard medical glass slide (with the size of 75 mm * 25 mm * 1 mm) and covered by a medical glass coverslip (with the size of 22 mm * 22 mm*0.1 mm). The medical glass coverslip is firmly close to the circular aperture. The bottom of the medical glass slide keeps the distance of ~500 μm, named as L_2, from the CMOS image sensor. Thus, the optical distance between the pathological tissue slice and the CMOS image sensor is ~2 mm. The ratio of L_1 and L_2 is ~300, thus the imaging magnification of the recorded hologram over the pathological tissue slide is ~1. Therefore, the illumination can be regard as a plane wave. As the diffraction patterns of the circular aperture need to be recorded totally, the diameter of the circular aperture should be less than the width of the CMOS image sensor. As shown in Fig. 1(a), the exit end of the optical fiber and circular aperture is fixed. The core diameter of the optical fiber is 600 μm. The diameter of the circular aperture is 4.8 mm, which is equivalent to 1000 pixels of the CMOS image sensor. The pathological tissue slide is fixed on a 3D-axial fine mechanical translation table with the resolution of ~10 μm. And the CMOS image sensor is also fixed on a 3D-axial fine mechanical translation table with the resolution of ~10 μm. The green LED is with the power of 3 W, provided by the JUXIANG Technology, CHINA. The green LED's dominant wavelength is 550 nm, with the spectral bandwidth of ~40 nm. The multi-mode quartz optical fiber is the CORE600UM, SHOULIANG Optics, CHINA. The 3D-axial fine mechanical translation table to support the pathological tissue slide is the XYZ60MM, JUXIANG Technology, CHINA. The 3D-axial fine mechanical translation table to support the CMOS image sensor is the XYZ25MM-C, JUXIANG Technology, CHINA. The CMOS image sensor is the MV-CB060–10UM-B/C/S, HIKVISION, CHINA, whose sensor is IMX178, with the pixel size of 2.4 μm and the resolution of 3072 ×2048. The pathological tissue slide is biologically and chemically processed in the bio-medical lab of Suzhou Municipal Hospital (SMH), following the de-identification of the basic clinical information, approved and supervised by the Medical Ethic Committee of SMH. Firstly, the tumor tissues are cut into thin slice with ~ 2–4 μm. Then, these tumor tissue slices are baked at 68 ˚C for 30 min and deparaffinized through xylene, absolute and 95% alcohols to distilled water. Thirdly, the sections are dyed with hematoxylin and eosin in turn, dehydrated through graded ethanol solutions and cleared with xylene. Finally, these H&E-stained slides are sealed with a half drop of neutral resin gum and covered with a coverslip.

The Fig. 2(a) is the schematic of our PIE lens-less microscopy. Different from Fraunhofer-diffraction PIE, our PIE lens-less microscopy is based on the Fresnel-diffraction. The gap between the pathological slide and the CMOS image sensor is only ~0.5–1 mm. The x-y coordinate/positions of the circular aperture and the CMOS image sensor are fixed. While the pathological tissue slide is precisely shifted along the x-y axis. These x-y shifts could be equivalent to the shifts of the circular aperture, which is presented in Fig. 2(b). The area overlap of each adjacent aperture couple is 80%. When the equivalent aperture is at the first position, the CMOS image sensor is moved along the z-axis as ~50 μm to record 2 different defocusing holograms, which are to execute the Transport-of-Intensity equation (TIE) solving for a complex-value initialization of PIE. Then, when the equivalent aperture is moved to a new x-y position, the related Fresnel-diffraction pattern is recorded by the CMOS image sensor. In the following part, we would introduce the computational algorithms to reconstruct a colorful PIE lens-less microscopy image.

3. Computational algorithm

3.1. PIE based on fresnel propagation

Flow charts of colorful PIE microcopy computational algorithms are shown in Fig. 3. The circular aperture is close to the pathological tissue slide, and the passed light after the circular aperture is named as a probe, which would be expressed as a complex-value function $P(r - R_{s(j)})$, where r represents $r(x, y)$, which means the objective point coordinates on the pathological tissue slide; $R_{s(j)}$ is the relative shift between the illumination area and the j-th shifted sample. The object is expressed as a complex-value function $O(r)$. The output wave's complex-value function is $\varphi_n(r, R_{s(j)}) = P(r - R_{s(j)}) \cdot O(r)$. The propagated diffraction wavefront is $Fresnel\{\varphi_n(r, R_{s(j)}), z\}$. The CMOS image sensor records the diffraction image, which is named as $I_{s(j)}$, where $I_{s(j)}$ is the s(j)-th recorded Fresnel diffraction pattern, and proportional to the squared modulus of the propagated diffraction wavefront, $I_{s(j)} \propto |Fresnel\{\varphi_n(r, R_{s(j)}), z\}|^2$. Afterwards, the chemically dyed pathological tissue slide is moved to a new position. At this new position, another part of the pathological tissue slide is illuminated and the intensity of the relative diffracted wavefront is recorded by the CMOS image sensor. In this manuscript, $R_{s(j)}$ is the relative vector shift between the pathological tissue slide and the probe. Based on the recorded diffracted images and computationally iteratively phase retrieval algorithm, the high-resolution microscopy image of the pathological tissue slide would be reconstructed. Different from the Fraunhofer diffraction, our computational iterations are based on the Fresnel diffraction. Besides, the initial guess of $O_0(r)$ could be provided by the TIE solving, based on two axial shift diffraction images [9–12]. The algorithms of the deep learning colorful PIE lens-less microscopy could be described in following steps:

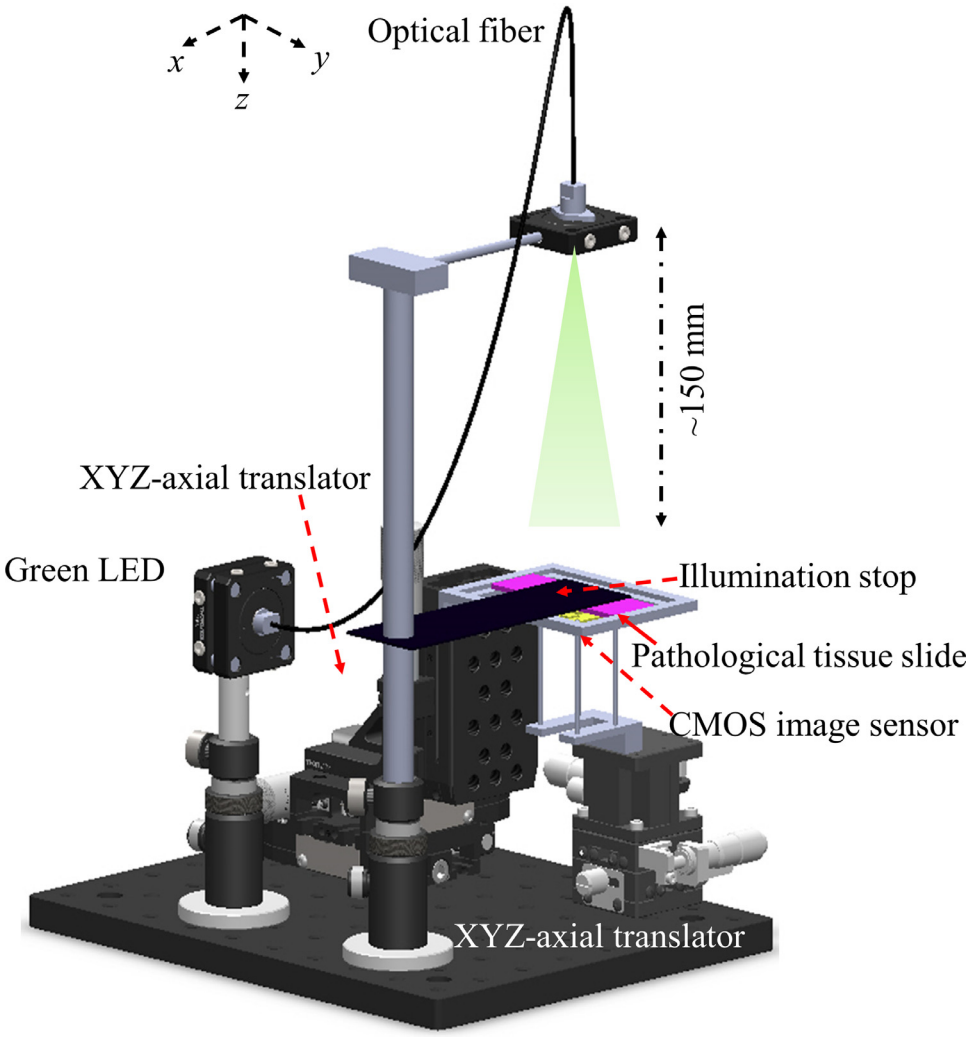

Fig. 1. The 3D structure of PIE lens-less microscopy experimental setup with an extensive field-of-view (FOV).

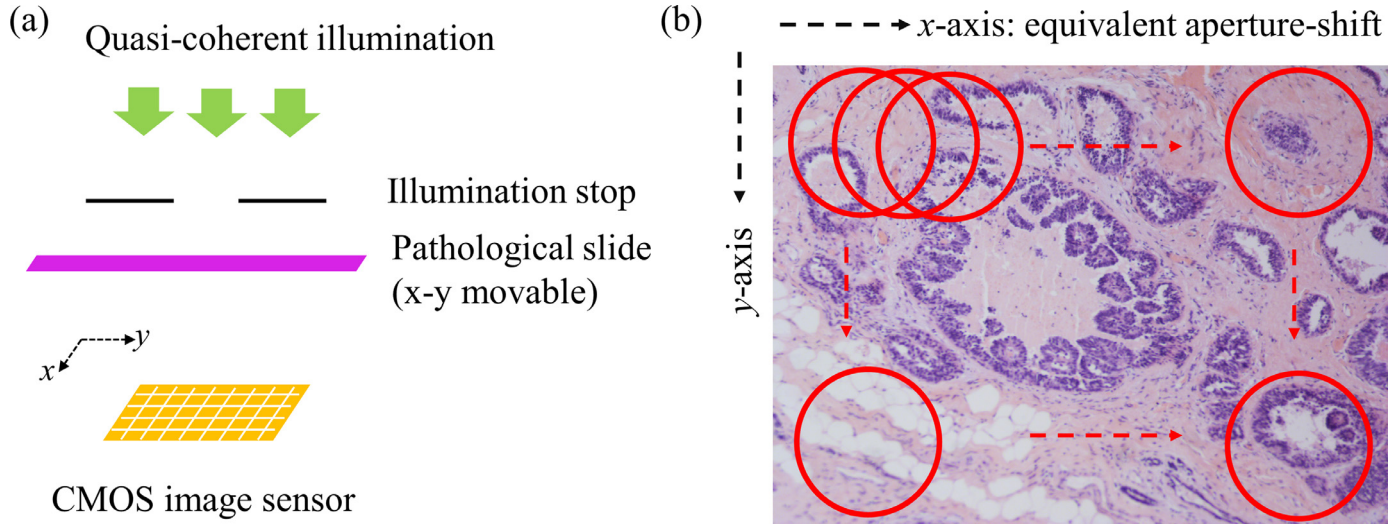

Fig. 2. Illumination ways of our PIE lens-less microscopy setup. (a) A 2D-schematic illustration about our PIE lens-less microscopy. (b) The equivalent aperture-shift illustration, where in practice the aperture and CMOS image sensor is fixed and the pathological tissue slide is moved.

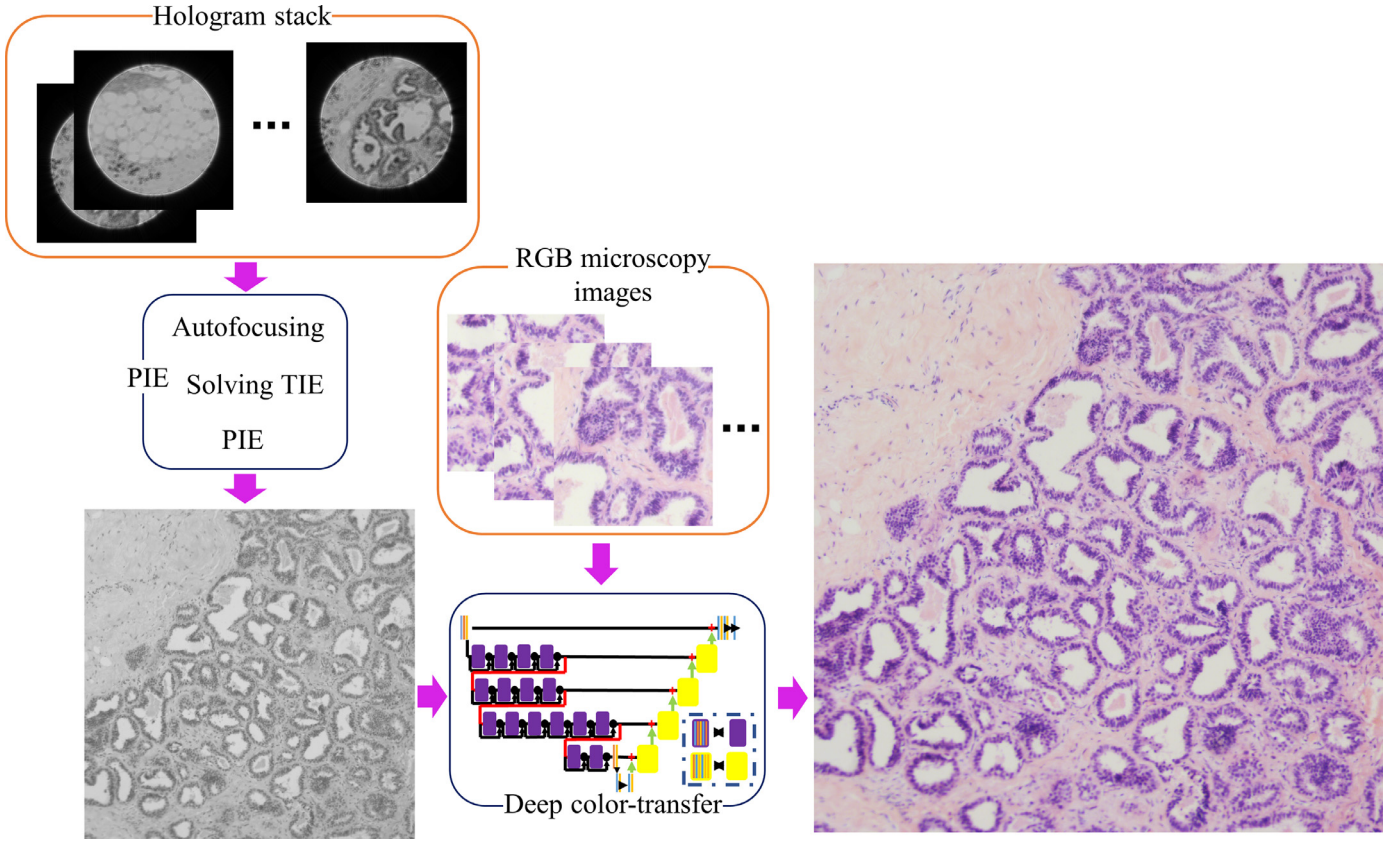

Fig. 3. Flow charts of computational algorithms for colorful PIE microcopy with only one kind illumination.

Step 1: The pathological tissue slide is initialized as $O_0(r)$ by the TIE solving; and the illumination probe on the pathological tissue slide, named as the object function, is initially guessed as $P(r - R_{s(0)})$. The initial guess of $P(r - R_{s(0)})$ is roughly the x-y region size of the illumination on the pathological tissue slide surface. The diffraction images of the pathological tissue slide are addressed in a stack $s(j)$.

Step 2: Beginning with the diffraction pattern $s(0)$, at the exit position after the pathological tissue slide, the complex initialization is the Eq. (1).

$$\varphi_n\left(r, R_{s(j)}\right) = O_n(r) \times P\left(r - R_{s(j)}\right), \tag{1}$$

where $O_n(r)$ is the object function, $P(r - R_{s(j)})$ is the equivalent shifted illumination probe guess.

Step 3: The complex-value $\varphi_n(r, R_{s(j)})$ is computationally propagated to the CMOS image sensor plane, as the Eq. (2).

$$\psi_n\left(u, R_{s(j)}\right) = Fresnel\left\{\varphi_n\left(r, R_{s(j)}\right), z\right\}, \tag{2}$$

where the $Fresnel\{*, z\}$ denotes the Fresnel wavefront propagation. The z at every position is determined by the computationally autofocusing method. The steps of computationally autofocusing are necessary and important, as the z-shift-errors occur when the pathological slide moves. And the Eq. (2) can be re-expressed as Eq. (3).

$$\psi_n\left(u, R_{s(j)}\right) = \left|\psi_n\left(u, R_{s(j)}\right)\right| \exp\left[j\theta_n\left(u, R_{s(j)}\right)\right]. \tag{3}$$

Step 4: The amplitude (real-value) of the $\psi_n(u, R_{s(j)})$ in Step (3) is substituted by the square root of the recorded diffracted pattern, while the phase information is kept. The Eq. (4) would be got from Eq. (3),

$$\psi_{c,n}\left(u, R_{s(j)}\right) = \sqrt{I_{s(j)}} \exp\left[j\theta_n\left(u, R_{s(j)}\right)\right], \tag{4}$$

Step 5: The Eq. (4) would be back-propagated to the object function, expressed as the Eq. (5)

$$\varphi_{c,n}\left(r, R_{s(j)}\right) = Fresnel^{-1}\left\{\psi_{c,n}\left(u, R_{s(j)}\right), z\right\}. \tag{5}$$

Step 6: The object function $O_{j+1}(r)$, and the illumination probe function $P_{j+1}(r)$ are updated as Eq. (6) and Eq. (7), respectively.

$$O_{j+1}(r) = O_j(r) + \alpha \frac{P_j^*\left(r - R_{s(j)}\right)}{\left|P_j\left(r - R_{s(j)}\right)\right|^2_{max}} \left(\varphi_{c,n} - \varphi_n\right), \tag{6}$$

$$P_{j+1}(r) = P_j(r) + \beta \frac{O_j^*\left(r + R_{s(j)}\right)}{\left|O_j\left(r + R_{s(j)}\right)\right|^2_{max}} \left(\varphi_{c,n} - \varphi_n\right), \tag{7}$$

where α and β are the adjustable iteration step parameters for convergence. The $O_{j+1}(r)$ is viewed as the newly updated 'guessed' object function, and $P_{j+1}(r)$ is viewed as the newly updated 'guessed' illumination probe function. Then, they are repeatedly executed as the Step (1) to the Step (6), based on the recorded diffraction pattern s(1), s(2),…, s(j), until all recorded diffraction patterns have been used to update the object and the probe guess. Up to now, one PIE iteration cycle is completed.

Step 7: Here we define a normalized RMS error metric function to measure the iteration as Eq. (8).

$$E_n = \frac{\sum_j \sum_u \left|\sqrt{I_{s(j)}} - \psi_n\left(u, R_{s(j)}\right)\right|^2}{\sum_j \sum_u I_{s(j)}}. \tag{8}$$

When the E_n is less than a given value, the iterations would be stopped. Otherwise, the iterations would be continued.

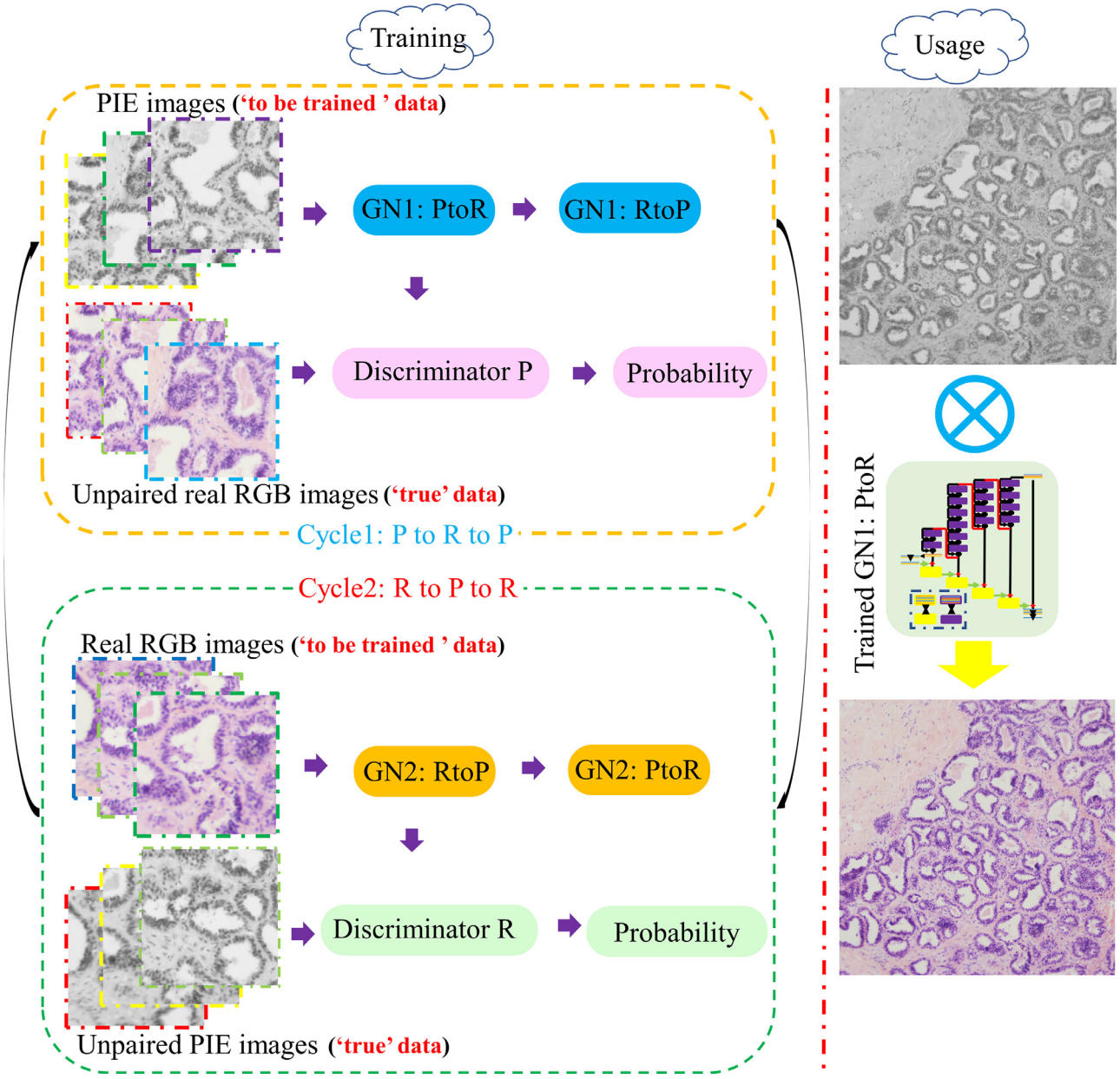

Fig. 4. A GAN framework to achieve deep-color transferring for PIE microscopy.

3.2. Deep learning color-transfer

Transferring photos in one picture style onto another picture style by computational deep learning methods, has been developed by several research groups [21–28]. These computational image-style-transferring methods have shown potentials for creating virtual oil artistic painting, virtual comic cartoon pictures/movies and virtual chemically dying. Inspired by these references [29–34], we design a deep learning network frame to achieve colorful PIE microscopy imaging under only one kind of illumination. Firstly, the images information is formated into YCbCr color space for deep-color transferring. Based on the idea of zero-sum competition game, we design a generative adversarial network (GAN) framework, as shown in Fig. 4. This GAN framework contains two kinds of interactive networks, i.e., the generator network (GN) and the discriminator network (DN). The input/output of the GN is matrix data with 3 channels as the picture format in YCbCr color space, which is named as the GN images. While the function of DN is to discriminate the GN images and the 'real' images. The input data of the DN are the 'real' images and the GN images, namely output data of the GN. The 'real' images are adopted by the commercial bench-top brightfield microscope (NIB900L, NOVEL, CHINA). By zero-sum-competition game to minimize both differences of colors and texture details, the DN would enforce the GN to generate images with both the desired textures and the desired colors, on the basis of gray-scale PIE lens-less microscopy amplitude images. The framework looks like a traditional Chinese Grate Ultimate/Taiji, combining two totally opposite into a harmony circle. In this manuscript, one is the gray-scale PIE lens-less microscopy image data, while the other is the real RGB conventional bright-field microscopy image data. In the training stage (Fig. 4), there are two training cycle to compete each other in a zero-sum-competing game. One is the 'Cycle1: P to R to P', where 'P' means the PIE lens-less microscopy images, and 'R' means the RGB conventional bright-field microscopy images. The other

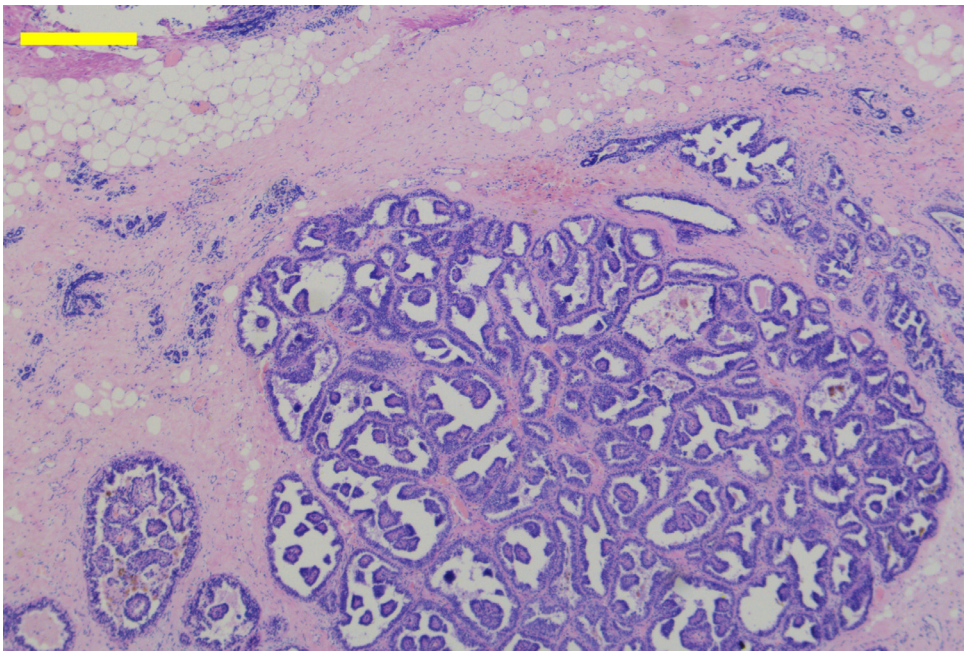

Fig. 5. A reconstructed colorful PIE microscopy image with a large FOV (12 mm * 7.9 mm). The yellow color scalebar is ~1.5 mm.

is the 'Cycle2: R to P to R', where 'R' and 'P' are the same meaning in the Cycle 1. For each generator network of Cycle1 and Cycle2, there is an independent discriminator network. As shown in Fig. 4, the Discriminator P aims to distinguish the generated images by the 'GN1: PtoR' with the unpaired real RGB images; while the Discriminator R aims to distinguish the generated images by the 'GN2: RtoP' with the unpaired real PIE lens-less microscopy images. In all generators, the architectures are the same, which have 8 layers including: Input Layer, Convolution Layer (stride 1, pad 3), Convolution Layer (stride 2, pad 1), Convolution Layer (stride 2, pad 1), 9 Consecutive Residual Blocks, Transpose Convolution Layer (stride 2, pad 1, out_pad 1), Transpose Convolution Layer (stride 2, pad 1, out_pad 1), and Convolution Layer (stride 1, pad 3). In all discriminators, the architectures are also the same, including: Input Layer, Convolution Layer (stride 2, pad 1), Convolution Layer (stride 2, pad 1), Convolution Layer (stride 2, pad 1), Convolution Layer (stride 1, pad 1), and Convolution Layer (stride 1, pad 1). Above architectures and layers are construct by the python language and TensorFlow (TF) framework version 2.1, under the Anaconda software environment (open source).

There is an advantage in our deep color-transferring GAN, where the digital image registration is not necessary. Thus, in the data preparatory stage, there are no computational image rescaling, computational image rotation and computational image registration, although the two image stacks data are from totally different optical imaging systems and digital image sensors. To keep the color information and the image texture details together harmoniously, like a traditional Chinese Grate Ultimate/Taiji, we designed a loss function as Eq. (9) to reserve the color and image texture and structural feature information.

$$Loss = L(GN1 : PtoR) + L(GN2 : RtoP) + L(cycle) + 0.1(1 - msSSIM(GN1, R)) + 0.1(1 - msSSIM(GN2, P)), \quad (9)$$

where $L(GN1 : PtoR)$ and $L(GN2 : RtoP)$ are the loss function for each couple of GN-DN respectively. $L(cycle)$ is the total cycle consistency loss. The 'msSSIM' represents the multiscale structural similarity index (SSIM) of the green channel. The last two expressions aim to keep structural and texture detail information [35]. In the color-transfer GAN, an adaptive moment estimation (Adam) optimizer was to update the network learnable parameters.

4. Results

Throughout experiments, diffraction pattern recording, PIE reconstruction and deep color transferring, the colorful PIE microscopy results are presented in Figs. 5–7. In computational environments, the deep learning virtually colorizing is processed on a desktop computer, which is with a Windows 10 operating system (Microsoft), a Core i7–7700 K CPU @ 4.2 GHz (Intel) and 64GB of RAM and dual GeForce GTX 1080Ti GPUs (NVIDA). The GAN is constructed by using TensorFlow (TF) framework version 2.1 and Python version 3.7. The learning rate is set as of 5×10^{-4} for the generator, in both the 'Cycle1: P to R to P' and the 'Cycle2: R to P to R'. In both independent discriminators, the learning rate is set as 1×10^{-6}. In the training stage, the images are all cropped into the digital size of 512×512 pixels. For training, we used 2048 unpaired image couples, and for testing, we used 256 unpaired image couples. The training convergences data are presented in the Table 1. The training time is ~40 h, where ~1.6 h are enough to get a good convergence (at the iteration of 200 in Table 1). In the usage stage, to transfer the cropped PIE lens-less microscopy image with the digital size of 512×512 pixels into a RGB colorful image, only ~7 ms are used in the same bench-top computer. Finally, the transferred colorful PIE lens-less microscopy images are matched together into a large resolution colorful PIE lens-less microscopy image.

In Fig. 5, it presents a reconstructed colorful PIE microscopy image with a large FOV (12 mm * 7.9 mm), while the resolution ability is ~3 μm. The FOV could be further improved. In our colorful PIE microscopy imaging, the diffraction patterns are collected under only G LED illumination. In Fig. 6, some colorful PIE microscopy images of randomly selected regions are presented. Each pair is ranged in the dash line rectangle: the left one is the original PIE microscopy image, which is greyscale; the middle one is the deep-learning colorful PIE microscopy image; the right one is the colorful brightfield microscopy image. The results show that our deep color-transferring method keep the details well for PIE microscopy imaging. In Fig. 7, the comparison stacks of the colorful PIE microscopy images and conventional RGB brightfield images. Based on 256 comparison pairs, we calculate the average value of the <DELTA E(94)> [36,37] performances, which is used as evaluate the color differences. The average value of the <DELTA E(94)>,

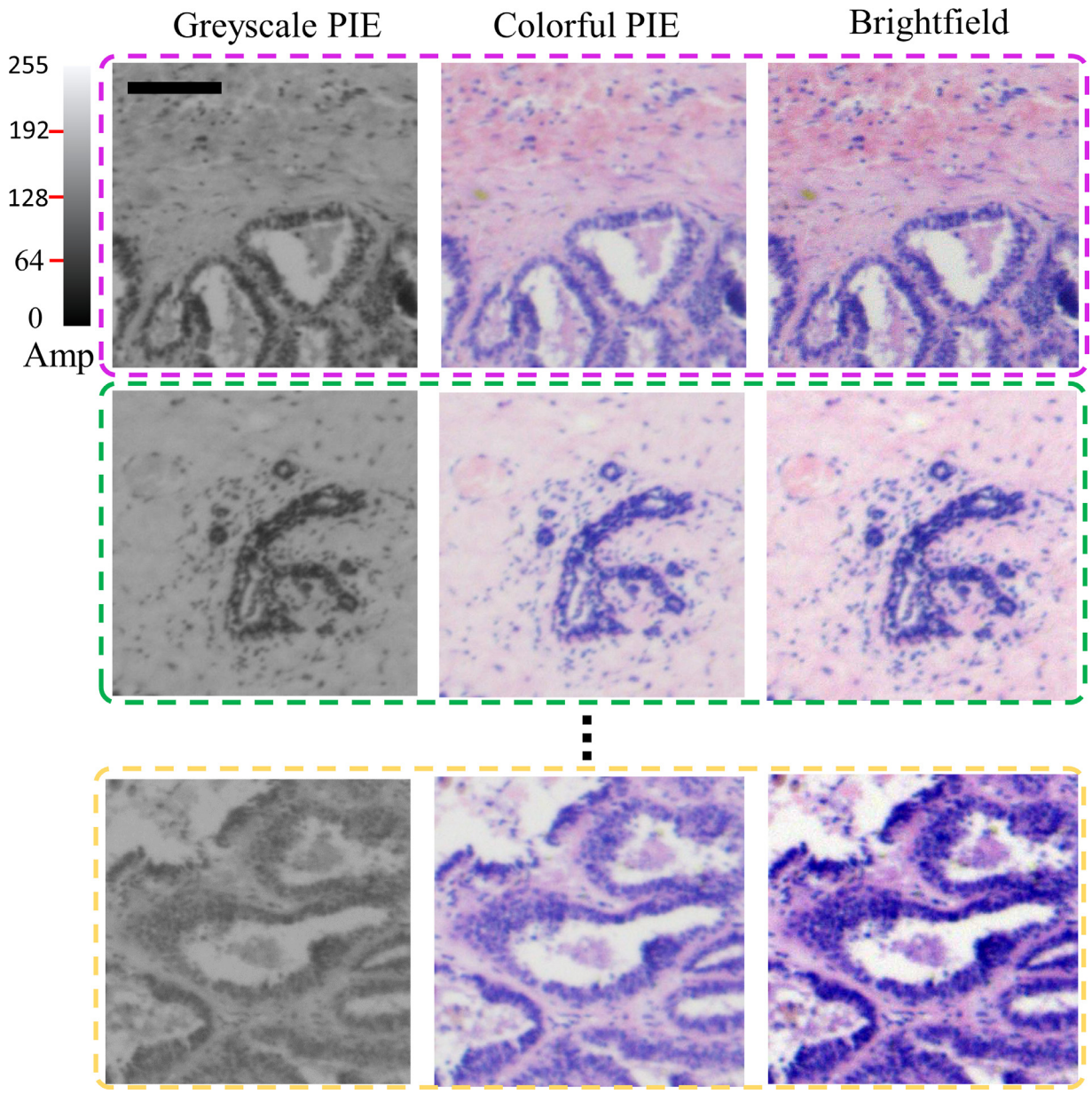

Fig. 6. Images pairs of origin greyscale PIE microscopy, colorful PIE microscopy and conventional RGB brightfield. The top-left black scale bar is about 200 μm. The amplitude images are with the greyscale of [0, 255].

Table 1
Training convergence data in the deep training stage.

Epoch	1	10	50	100	200	500	1000	5000
Loss	0.751	0.206	0.1272	0.1253	0.1241	0.1241	0.1241	0.1241

between our colorful PIE images and the conventional RGB brightfield images, is 2.7105, which means the color difference is narrow [,37]. After deep trained, the deep color-transferring is very fast, which is ~7 ms under our bench-top computer. However, the execution time of PIE process is very long, whose total computational time is ~30 min, where includes autofocusing, TIE and PIE. All of their algorithms have a lot of Fourier transforms, iterations and maximum/minimum local researching methods. Thus, our deep color-transferring methods almost do not aggravate the burden of the total PIE microscopy imaging time.

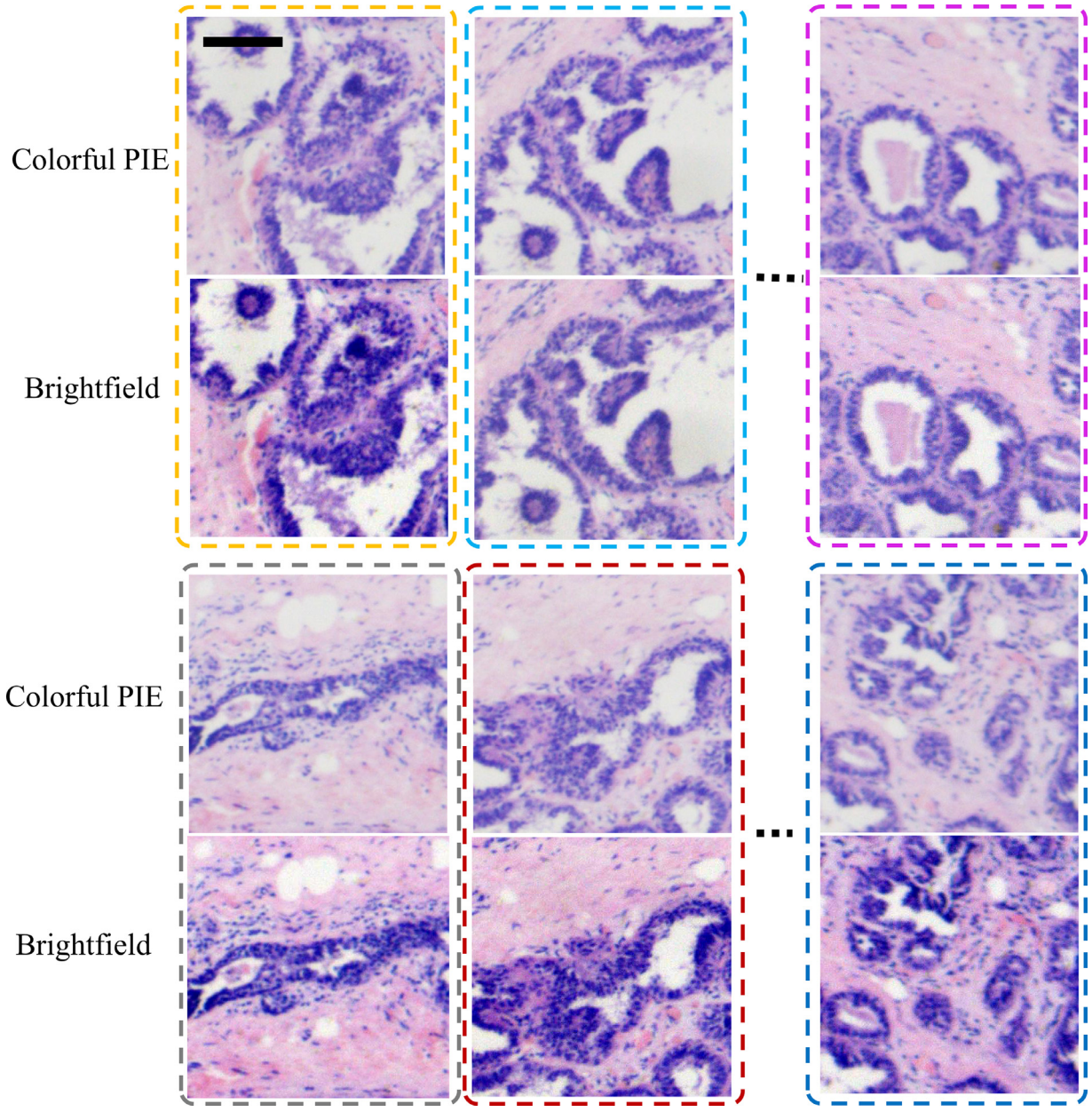

Fig. 7. Vision comparisons of colorful PIE microscopy images and conventional RGB brightfield images. The top-left black scale bar is about 200 μm.

5. Conclusion

In this manuscript, a computational color-transfer method based on deep learning, is proposed to enhance the PIE lens-less microscopy. The PIE lens-less microscopy setup under only one quasi-chromatic light illumination, would achieve colorfully microscopy imaging. In the traditional colorful PIE microscopy setups, more than three kinds of different wavelengths are used to get a RGB image. This deep color-transfer method broadens the attractiveness and application of the PIE lens-less microscopy, which would benefit the development of low-cost large FOV microscopes. Our color-transfer deep learning network is trained on the basis of the H&E-stained pathological tissue slides. The deep learning color-transfer method would work for other staining medical diagnosis, e.g., fluorescent staining, Sudan staining and so on. By the experiments and data, we present that the deep learning color-transfer method work well on a PIE lens-less microscopy setup under only G LED illumination, which proves the effectiveness and robustness of the proposed concept. Thus, it is believable that our colorful PIE microscopy enhanced by the deep learning color-transfer method would be helpful for the development of low-cost large FOV lens-less microscopes. We also believe our deep color-transfer method also is fit for other quasi-chromatic illumination microscopy setups.

Data availability statement

The data that support the findings of this study are available from the corresponding author upon reasonable request.

Author statement

Cuifang Kuang and Hua Shen proposed the initial ideas. Yinxu Bian coded the python scripts. Yinxu Bian and Weijie deng built the PIE experimental setup and recorded the original hologram data. Yannan Jiang and Jiaxiong Wang prepared the pathological tissue slide samples. Shenmin Yang and Renbing Shen supervised the medical biosample preparation. Yinxu Bian, Weijie Deng and Xiaofei Yang prepared the manuscript.

All authors contributed to the manuscript. Cuifang Kuang and Hua Shen supervised the research.

For data and code availability, anyone, who is interested in our research, could contact the Cuifang Kuang and Hua Shen for the original data and code scripts.

Declaration of Competing Interest

All authors declare that they have no conflict of interest.

Acknowledgement

This study is partially supported by National Natural Science Foundation of China (NSFC) (62005120), the Basic Research Program of Jiangsu Province (BK20190456, BK20201305), the Fundamental Research Funds for the Central Universities (30919011261), Beijing Satellite Environmental Engineering Institute (CAST-BISEE2019–038), Chinese Academy of Sciences (KLOMT190101), Suzhou Science and Technology Development Project (SYSD2020132) and the National Key Research and Development Program (2019YFB2005500).

References

[1] Hoppe W. Diffraction in inhomogeneous primary wave fields: 1. principle of phase determination from electron diffraction interference. Acta Crystallogr A 1969;25:495–501.
[2] Rodenburg John M. Ptychography and related diffractive imaging methods. Advan imag electron phys 2008;150:87–184.
[3] Pfeiffer F. X-ray ptychography. Nature Photon 2018;12:9–17.
[4] Seaberg MD, Zhang B, Gardner DF, Shanblatt ER, Murnane MM, Kapteyn HC, Adams DE. Tabletop nanometer extreme ultraviolet imaging in an extended reflection mode using coherent fresnel ptychography. Optica 2014;1:39.
[5] Valzania L, Feurer T, Zolliker P, Hack E. Terahertz ptychography. Opt Lett 2018;43:543.
[6] Maiden AM, Rodenburg JM. An improved ptychographical phase retrieval algorithm for diffractive imaging. Ultramicroscopy 2009;109:1256.
[7] Pan A, Zuo C, Yao B. High-resolution and large field-of-view fourier ptychographic microscopy and its applications in biomedicine. Rep Prog Phys 2020;83:096101.
[8] Yuting G, Jiurun C, Aiye W, An P, Caiwen M, Baoli Y. High-throughput fast full-color digital pathology based on fourier ptychographic microscopy via color transfer. SCIENCE CHINA: Physics, Mechanics & Astronomy 2021.
[9] Guo C, Wei C, Tan J, Chen K, Liu S, Wu Q, Liu Z. A review of iterative phase retrieval for measurement and encryption. Opt Lasers Eng 2017;89:2–12.
[10] Sun A, Jiang Z, Kong Y, Xue L, Wang S, Liu C. Multi-probe ptychographic iterative engine method. Opt Commun 2019;436:174–9.
[11] Dou J, Gao Z, Ma J, Yuan C, Yang Z, Claus D, Zhang T. Phase retrieval based on pupil scanning modulation. Appl Phys B 2017;123:217.
[12] Dou J, Zhang T, Wei C, Yang Z, Gao Z, Ma J, Li J, Hu Y, Zhu D. Single-shot ptychographic iterative engine based on chromatic aberrations. Opt Commun 2019;440:139–45.
[13] Zuo C, Li J, Sun J, Fan Y, Zhang J, Lu L, Zhang R, Wang B, Huang L, Chen Q. Transport of intensity equation: a tutorial. Opt Lasers Eng 2020:106187.
[14] Xin L, Liu X, Yang Z, Zhang X, Gao Z, Liu Z. Three-dimensional reconstruction of super-resolved white-light interferograms based on deep learning. Opt Lasers Eng 2021;145:106663.
[15] Liu X, Yang Z, Dou J, Liu Z. Fast demodulation of single-shot interferogram via convolutional neural network. Opt Commun 2021;487:126813.
[16] Niu M, Luo G, Shu X, Qu F, Zhou S, Ho Y-P, Zhao N, Zhou R. Portable quantitative phase microscope for material metrology and biological imaging. Photon. Res. 2020;8:1253–9.
[17] He W, Dou J, Yang Z, Liu Z, Liu Z. Sequential shift absolute phase aberration calibration in digital holographic phase imaging based on chebyshev polynomials fitting. IEEE Photonics J 2020;12:1–11.
[18] Zhu J, Zhou R, Zhang L, Ge B, Luo C, Goddard LL. Regularized pseudo-phase imaging for inspecting and sensing nanoscale features. Opt Express 2019;27:6719–33.
[19] Renjie Z, Di J, Zahid Y, Peter S. A portable quantitative phase microscope (Conference presentation). In: Proc.SPIE; 2018.
[20] An P, Yan Z, Tianyu Z, Zhaojun W, Dan D, Ming L, Baoli Y. System calibration method for fourier ptychographic microscopy. J Biomed Opt 2017;22:1–11.
[21] Zuo Z, Xu Q, Zhang H, Wang Z, Chen H, Li A, Zhao L, Xing W, Lu D, Multimodal image-to-image translation via mutual information estimation and maximization, 2020, arXiv:2008.03529.
[22] Touvron H, Douze M, Cord M, Jégou H,, Powers of layers for image-to-image translation, 2020, arXiv:2008.05763.
[23] Abraham T, Shaw A, O'Connor D, Todd A, Levenson R, Slide-free muse microscopy to h&e histology modality conversion via unpaired image-to-image translation gan models, 2020, arXiv:2008.08579.
[24] Shaban MT, Baur C, Navab N, Albarqouni S. Staingan: stain style transfer for digital histological images. In: 2019 IEEE 16th international symposium on biomedical imaging (ISBI 2019); 2019. p. 953–6.
[25] Tao X, Zhang J, Sun P, Wang C, Tao C, Wu R, Zheng Z. Phase-coded speckle illumination for laser fourier ptychographic microscopy. Opt Commun 2021:127199.
[26] Liu T, Wei Z, Rivenson Y, de Haan K, Zhang Y, Wu Y, Ozcan A. Deep learning-based color holographic microscopy. J Biophotonics 2019;12:e201900107.
[27] Manwar R, Li X, Mahmoodkalayeh S, Asano E, Zhu D, Avanaki K. Deep learning protocol for improved photoacoustic brain imaging. J. Biophotonics. 2020;13:e202000212.
[28] Manwar R, Li X, Mahmoodkalayeh S, Asano E, Zhu D, Avanaki K. Improved photoacoustic brain imaging using a deep learning protocol. Photons Plus Ultrasound: Imaging and Sensing 2021:11642.
[29] Liang H, Plataniotis KN, Li X, Stain style transfer of histopathology images via structure-preserved generative learning, 2020, arXiv:2007.12578.
[30] Shen J, Chen Y, Ding Z, Chang S, Tao C, Wu F, Li Y, Zheng Z. Development of energy correction based multishot snapshot spectral imaging system. Opt Commun 2019;432:116–22.
[31] Shen J, Chang S, Wang H, Zheng Z. Optimal illumination for visual enhancement based on color entropy evaluation. Opt Express 2016;24:19788–800.
[32] Tao X, Zhang J, Tao C, Sun P, Wu R, Zheng Z. Tunable-illumination for laser fourier ptychographic microscopy based on a background noise-reducing system. Opt Commun 2020;468:125764.
[33] Rivenson Y, de Haan K, Wallace WD, Ozcan A. Emerging advances to transform histopathology using virtual staining. BME Frontiers 2020;2020:9647163.
[34] Haan Kd, Rivenson Y, Wu Y, Ozcan A. Deep-Learning-Based image reconstruction and enhancement in optical microscopy. Proc IEEE 2020;108:30–50.
[35] Wang Z, Simoncelli EP, Bovik AC. Multiscale structural similarity for image quality assessment. In: The thrity-seventh asilomar conference on signals, systems & computers; 2021. p. 1398–402.
[36] https://en.wikipedia.org/wiki/Color_difference. 2021.
[37] Hill B, Vorhagen FW, Roger T. Comparative analysis of the quantization of color spaces on the basis of the cielab color-difference formula. ACM Trans Graph 1997;16(2):109–54.